Lightning Enhancement Over Major Oceanic Shipping Lanes

Joel A. Thornton[1], Katrina S. Virts[2], Robert H. Holzworth[3], and Todd P. Mitchell[4]

[1]Department of Atmospheric Sciences, University of Washington, Seattle, Washington

[2]NASA Marshall Space Flight Center, Huntsville, Alabama

[3]Department of Earth and Space Sciences, University of Washington, Seattle, Washington

[4]Joint Institute for the Study of the Atmosphere and Ocean, University of Washington, Seattle, Washington

Corresponding author address: thornton@atmos.uw.edu

Key Points

- **Lightning is enhanced by about a factor of two directly over two of the busiest shipping lanes in the Indian Ocean and South China Sea**
- **Environmental factors such as convergence, sea surface temperature, or atmospheric stability do not explain the enhancement**
- **We hypothesize shipping emissions of particles change storm cloud microphysics, enhancing condensate in the mixed phase region and thus lightning.**

This article has been accepted for publication and undergone full peer review but has not been through the copyediting, typesetting, pagination and proofreading process which may lead to differences between this version and the Version of Record. Please cite this article as doi: 10.1002/2017GL074982

Abstract

Using twelve years of high resolution global lightning stroke data from the World Wide Lightning Location Network (WWLLN), we show that lightning density is enhanced by up to a factor of two directly over shipping lanes in the northeastern Indian Ocean and the South China Sea as compared to adjacent areas with similar climatological characteristics. The lightning enhancement is most prominent during the convectively active season, November-April for the Indian Ocean and April-December in the South China Sea, and has been detectable from at least 2005 to the present. We hypothesize that emissions of aerosol particles and precursors by maritime vessel traffic lead to a microphysical enhancement of convection and storm electrification in the region of the shipping lanes. These persistent localized anthropogenic perturbations to otherwise clean regions are a unique opportunity to more thoroughly understand the sensitivity of maritime deep convection and lightning to aerosol particles.

Introduction

Lightning results from the electrification of cumulonimbus cloud systems formed during deep convective storms, and is measured globally by land-based networks and satellite sensors in part for its utility as an indicator for storm intensity and vertical development.[*Williams*, 2005] Lightning directly alters atmospheric composition through the formation of nitric oxide radicals in the high temperature plasma.[*Price et al.*, 1997] Nitrogen oxides regulate the oxidizing capacity of the atmosphere,[*Logan*, 1983] influence the abundance and lifetimes of trace gases important for the greenhouse effect,[*Mickley et al.*, 2001; *Stevenson et al.*, 2013] and are a major source of fixed nitrogen useful to the biosphere.[*Galloway et al.*, 2004] Lightning strikes cause loss of human life and property,[*Curran et al.*, 2000] and perturb ecosystems through wildfire ignition.[*Flannigan and Wotton*, 1991; *Rorig and Ferguson*, 1999] As such, determining whether storm intensity and lightning frequency have changed, or will change, due to human activities, remains an important research objective for many disciplines.[*Seiler and Crutzen*, 1980; *Price et al.*, 1997; *Mickley et al.*, 2001]

Cloud electrification, and thus lightning, requires ice formation to occur within the cloud,[*Reynolds et al.*, 1957; *Sherwood et al.*, 2006] which in turn requires deep convection of sufficient water mass to high altitudes where temperatures are well below the freezing point of water. Fulfillment of these requirements depends upon the thermodynamic structure of the troposphere as well as the microphysics of the cloud.[*Williams et al.*, 2002; *Mansell and Ziegler*, 2013; *Stolz et al.*, 2015] Low concentrations of cloud condensation nuclei (CCN), suspended solid or liquid aerosol particles greater than about 50 nm in size, lead to clouds with larger droplets more susceptible to coalescence into warm rain and dissipation before reaching glaciation conditions.[*Rosenfeld et al.*, 2014] Higher CCN concentrations lead to more numerous but smaller cloud drops,[*Ramanathan et al.*, 2001] which leads to

suppressed or delayed warm rain formation, and thus potentially more water transported to the colder upper atmosphere if continued uplift is sustained by dynamics or thermodynamics.[*Rosenfeld and Woodley*, 2000] Ice formation can further enhance convection due to the release of the latent heat of freezing, induce mixed-phase precipitation and lead to charge separation.[*Mansell and Ziegler*, 2013]

The above microphysical effect, known as aerosol convective invigoration,[*Koren et al.*, 2005] results in a potential sensitivity of lightning and storm vertical development to human activities, which have perturbed CCN concentrations on regional and global scales.[*Boucher and Lohmann*, 1995; *Pierce et al.*, 2007; *Merikanto et al.*, 2009; *Dunne et al.*, 2016] Aerosol invigoration of storms is found using computer models of cloud systems,[*Fan et al.*, 2013; *Mansell and Ziegler*, 2013; *Altaratz et al.*, 2014; *Rosenfeld et al.*, 2014; *Wang et al.*, 2014; *Zhao et al.*, 2014; *Guo et al.*, 2016] and observations often show positive correlations between cloud top height, and/or the lightning flash rate with aerosol optical depth (AOD), a proxy for CCN,[*Andreae*, 2004] or with below-cloud particle number concentrations.[*Andreae*, 2004; *Koren et al.*, 2005; *Bell et al.*, 2008, 2009; *Khain et al.*, 2008; *Altaratz et al.*, 2010; *Yuan et al.*, 2011; *Li et al.*, 2011; *Heiblum et al.*, 2012; *Wall et al.*, 2014; *Storer et al.*, 2014; *Stolz et al.*, 2015]

Over wider geographical areas, a causal relationship between CCN and lightning or convection can be harder to establish. CCN observations are rare and of limited spatial coverage and CCN, AOD and lightning flash rates are low over remote ocean regions [*Williams and Stanfill*, 2002]. CCN or AOD and dynamical forcing of convection are also often spatially correlated, such as between land and ocean regions [*Williams and Stanfill*, 2002]. Moreover, the responses of convection, lightning and precipitation to CCN are non-linear, saturating or even being suppressed at very high CCN.[*Rosenfeld*, 2000; *Rosenfeld et al.*, 2008; *Altaratz et al.*, 2010; *Stolz et al.*, 2015; *Guo et al.*, 2016]

We present a statistical analysis of lightning frequency over two of the world's busiest shipping lanes. Lightning is persistently enhanced directly over these shipping lanes, situated in regions with some of the highest climatological rainfall rates on Earth. Ship exhaust is known to be a major local perturbation to CCN over the remote oceans, leading to "ship tracks", low-level clouds formed or optically brightened by CCN from the ships.[*Twohy et al.*, 1995; *Durkee et al.*, 2000; *Hobbs et al.*, 2000; *Lauer et al.*, 2007; *Peters et al.*, 2011] We discuss the connection to aerosol convective invigoration and conclude that these areas will be useful to quantify the sensitivity of remote tropical marine convection and lightning to CCN.

Methods and Data

The World Wide Lightning Location Network (WWLLN; see http://wwlln.net) is the longest running global lightning network, with coverage beginning in August 2004. Analysis in this paper is based on over 1.5×10^9 individual strokes detected during 2005-2016. WWLLN locates lightning using dozens of radio receivers in the very low frequency range (VLF; 3-30 kHz) located throughout the world. Detected waveforms from each lightning sferic are used to calculate the time of group arrival (TOGA;[*Dowden et al.*, 2002]), and a minimum of five TOGAs, each from a separate WWLLN station, are used for time of arrival location determination. Timing accuracy is maintained by GPS receivers with 100 ns accuracy, and the lightning locations are accurate to within about 5 km [*Abarca et al.*, 2010; *Hutchins et al.*, 2012]. WWLLN detects the majority of all lightning-producing storms, even in regions with no stations within 2,000 km [*Jacobson et al.*, 2006; *Rodger et al.*, 2006]. While the number of thunderstorms detected by WWLLN has remained approximately level [*Hutchins et al.*, 2014], WWLLN's stroke detection efficiency has more than doubled as sensors were added to the network. Because of this trend in the detection efficiency, we

compare lightning statistics over the shipping lanes with those for adjacent regions having comparable WWLLN coverage.

We use estimates of shipping emissions from version 4.3.1 Emissions Database for Global Atmospheric Research (EDGAR, http://edgar.jrc.ec.europa.eu/overview.php?v=431 [*Crippa et al.*, 2016]), available as monthly averages for the year 2010 at 0.1^{o} resolution. These emissions estimates use fuel usage statistics based on real-time ship information (number, size/type, heading, speed, etc) from the Automatic Identification System (AIS) required on all marine vessels for collision avoidance, together with published ship emission factors [e.g., *Lack et al.*, 2009] to calculate mass emissions of aerosol particle types ($PM_{2.5}$, organic carbon, black carbon, etc) as well as gaseous precursors such as SO_2. More information on the emissions inventory and marine vessel traffic can be found in the Supplemental Information (SI).

AOD over the ocean is obtained from the Moderate Resolution Imaging Spectroradiometer (MODIS; collection 6, level 2 [*Remer et al.*, 2008]). Aerosol backscatter vertical profiles (version 4, level 2 data) are measured by the Cloud Aerosol Lidar with Orthogonal Polarization (CALIOP) aboard the CALIPSO satellite [*Winker et al.*, 2007]. We also use radar reflectivity and lightning flash rates observed respectively by the Precipitation Radar (PR; dataset 2A25, version 7; [*Iguchi et al.*, 2000]) and the Lightning Imaging Sensor (LIS; version 4; [*Boccippio et al.*, 2002]) aboard the Tropical Rainfall Measurement Mission (TRMM) satellite, and 3-hourly gridded rain rates estimated from TRMM and other microwave and infrared satellite sensors (dataset 3B42, version 7; [*Huffman et al.*, 2007]). Characteristics of the large-scale thunderstorm environment are taken from the European Centre for Medium-Range Weather Forecasts (ECMWF) interim re-analysis (ERA-Interim), whose assimilated variables include ship weather observations [*Dee et al.*, 2011]. Daily sea surface temperatures (SST) at 0.25^{o} resolution are taken from the NOAA Optimal

Interpolation (SST) dataset (OI SST, version 2, [*Reynolds et al.*, 2007; *Banzon and Reynolds*, 2017]), which includes both satellite and *in situ* ship observations.

Results and Discussion

WWLLN lightning density over southeastern Asia (Fig. 1a, plotted on a 0.1° × 0.1° grid, or about 10 × 10 km) shows lightning enhancements oriented along the narrow, heavily trafficked shipping lane around 6°N in the northeastern Indian Ocean, as well as a somewhat broader enhancement running from Singapore northeast into the South China Sea. For comparison, shipping emissions of aerosol particles less than 2.5 micrometers in size (PM2.5) from the EDGAR database are shown in Fig. 1b on a 0.1° × 0.1° grid. Emissions are calculated from global shipping activity and fuel consumption records together with emission factors measured per kg of fuel burned from various ship types. The shipping emissions data, and marine vessel automated information system (AIS) data,[*Smith et al.*, 2014] indicate that most vessels traversing the northern Indian Ocean follow a very narrow (<0.5^{o} wide), nearly straight track around 6°N between the southern end of Sri Lanka and the northern tip of Sumatra (see SI). East of Sumatra, the shipping lane runs southeast through the Strait of Malacca, rounding Singapore and extending northeast across the South China Sea, with a smaller second branch splitting off near the southern coast of Vietnam. Aerosol particle emissions in these shipping lanes are larger by an order of magnitude or more than in other shipping lanes in this region (as shown in Figure 1b), and are among the largest globally.

The lightning enhancement over shipping lanes is most pronounced in a relative sense away from land areas, where diurnal cycles in sea breezes and terrain-induced convergence can strongly modulate thunderstorm development and thus lightning frequency [*Virts et al.*, 2013]. Therefore, while lightning also occurs frequently over the Strait of Malacca, e.g., we focus on the open-ocean shipping lanes, and especially that over the Indian Ocean, where the

meteorological conditions are more homogeneous. We quantify the shipping lane enhancement of lightning and temporal variability, and then suggest mechanisms which may account for the observations.

To quantify the lightning enhancement and its temporal variations, we analyze 12 years of lightning location data and define reference regions adjacent and parallel to the main shipping lanes (Fig. 2a). Two reference regions in the Indian Ocean, one north and one south of the shipping lane, were averaged together for the background comparison. For the narrower South China Sea, one parallel reference region was defined to the east southeast. The relative detection efficiency of the WWLLN network is slowly varying in space,[*Hutchins et al.*, 2013] with negligible differences across the region in Fig. 1 [*Hutchins et al.*, 2012], and the diurnal occurrence of lightning is similar in both the shipping lanes and their parallel reference regions [*Virts et al.*, 2013]. Thus, temporal variations of lightning density over the shipping lanes can be directly compared to that over the adjacent reference regions of the Indian Ocean and South China Sea.

Daily time series of WWLLN lightning density over each shipping lane and reference region are shown in Fig. 2b-e after smoothing using 91-day and 731-day (2-year) running mean filters. WWLLN's increasing detection efficiency over time produces upward trends in lightning density for each region. However, lightning occurrence over the shipping lanes is clearly and persistently enhanced compared to the background rates in the adjacent reference regions, which would have the same trend in detection efficiency, even in 2005 when WWLLN's detection efficiency was lowest. The 91-day running means (panels b and d) show the normal annual variation of lightning activity in the regions due to the seasonal meridional migration of the inter-tropical convergence zone [*Waliser and Gautier*, 1993]. During the broad annual peak of the thunderstorm activity—November through April over

the Indian Ocean and April through December over the South China Sea—lightning over the shipping lanes is typically more than a factor of two higher than in the reference regions.

In 2-year running means, the polluted shipping lanes exhibit elevated lightning counts by 20 to 100% compared to the reference regions, with the separation growing somewhat larger over time, especially in the South China Sea lane, suggesting an increasing perturbation to lightning frequency in the shipping lane. Using port activity records, we show that the tonnage carried by marine vessels in and out of Singapore nearly doubled over the same period (see SI).

To further determine the spatial parameters of the regions with enhanced lightning activity, we focus on the more spatially isolated Indian Ocean shipping lane. Because this shipping lane is approximately zonal along 6°N, its variations can be evaluated using zonally averaged fields over the gray outlined box in Fig. 2a. Figure 3a shows integrated lightning density across the shipping lane for two-year periods, with 0.1° resolution in latitude and scaled by the maximum lightning density in each two-year period. The enhancement at 6°N is evident consistently throughout the 12-year record.

As shown in Fig. 2b, lightning over the Indian Ocean shipping lane exhibits a strong seasonal cycle. Zonally averaged lightning density in two seasons, November – April and May – October, are shown in Fig. 3b. The months November – April (blue line) encompass the most active regional lightning as the inter-tropical convergence zone (ITCZ) shifts southward. This season clearly shows a pronounced peak in lightning centered on the shipping lane at 6°N. During boreal summer, the ITCZ shifts northward in association with the South Asian monsoon, and during this period lightning density increases to the north of the shipping lane, although a relative maximum still exists over the shipping lane. The integrated shipping emissions of PM2.5 from the EDGAR model over the same region are shown in Fig. 3c. The shipping emissions, which do not account for subsequent transport by

the winds, are dominated by a prominent peak narrower than 0.5^{o} latitude that aligns spatially with the peak lightning enhancement and that varies in intensity by less than 10% over the year.

In Fig. 3d, we show the zonal mean Convective Available Potential Energy (CAPE), a quantity related to the potential thunderstorm updraft strength. While these CAPE values are uncertain due to a lack of observational constraints on upper tropospheric temperature profiles in the region, they do support the presence of numerous thunderstorms with no strong instability region coincident with the lightning enhancement. When the lightning enhancement is largest, CAPE varies smoothly from 450 to 500 J kg^{-1} between 5 and 7^{o}N. The boreal summer CAPE values are similarly smoothly varying (<10% variations) across the shipping lane, but increase northward of the shipping lane following summer insolation (see SI). Typical thunderstorms occur in environments with instability measured by CAPE higher than these values (i.e. > 1000 J kg^{-1}) [*Lucas et al.*, 1994]. In the SI, we show that zonal mean SST, an additional measure of thermodynamic forcing, also smoothly varies across the lightning enhancement region. Moreover, we analyzed the diurnal cycle of lightning (see SI), and the relative enhancement over the shipping lane is similar regardless of local time of day. Vertical wind shear and low-level convergence in the region show no detectable variations across the shipping lane. Thus, there is no persistent instability or forcing favoring enhanced convection coincident with the Indian Ocean shipping lane which could account for the lightning enhancement.

Ruling out natural enhancements to convection along the shipping lane, the remaining mechanisms leading to enhanced lightning in the vicinity of large shipping lanes involve, (*1*) ships in a convectively active region serving as attachment points, such that electrical breakdown (lightning) during storms is more frequent, or (*2*) aerosol particles from the ships' exhaust indirectly enhancing lightning production through perturbation of storm cloud

microphysics and electrification processes. Given that the actual widths of the shipping lanes are significantly narrower than the observed lightning enhancement (see SI), it is unlikely that lightning strikes to ships, or other localized ship effects,[*Voropayev et al.*, 2012] can explain the observed enhancement, and instead there is an atmospheric component, such as daily and weekly shifts in horizontal advection and convection, that spatially diffuses the lightning enhancement by maritime vessel traffic. We conclude that aerosol particles resulting from ship exhaust enhance CCN, which invigorate convection and ice processes above the shipping lanes, leading to enhanced lightning. In the SI, we show that ship emissions are likely a significant perturbation to CCN in the region of the shipping lanes.

Consistent with this idea, in Figure 4 we show vertical profiles of zonal mean radar reflectivity anomalies in precipitating storms for the same region in Figure 3, as measured by the TRMM satellite between November and April from 1998 – 2015. While noisy, upper level reflectivity is enhanced with 0.5 dBz anomalies extending to higher altitudes and approximately centered about 6^{o} N, supporting more convection and greater condensed phase water in the mixed-phase region over the Indian Ocean shipping lane (Figure 4a). Rain rates measured by TRMM and other sensors decrease smoothly from the equatorial region across the shipping lane to the north (Figure 4b). The limited sampling of the region by the TRMM satellite compared to the WWLLN lightning data prevents a further comparison of the temporal variations, though we note that flash rates from the TRMM Lightning Imaging Sensor show a lightning enhancement coincident with the shipping lane (see SI). The LIS enhancement is slightly broader spatially and larger in magnitude than that from WWLLN, possibly because of LIS' ability to detect more numerous but weaker intracloud flashes.

Most previous studies of aerosol effects on lightning have utilized remote sensing techniques to correlate aerosol optical depth (AOD) with lightning flash rate over specific regions.[*Koren et al.*, 2005; *Jenkins and Pratt*, 2008; *Khain et al.*, 2008; *Abarca et al.*, 2010;

Altaratz et al., 2010; *Yuan et al.*, 2011; *Heiblum et al.*, 2012; *Storer et al.*, 2014; *Wall et al.*, 2014; *Guo et al.*, 2016] These studies have typically found positive correlations, but weak or even negative correlations are also reported; in addition the effects of CCN on cloud microphysics, convection and electrification are nonlinear and can saturate.[*Rosenfeld*, 2000; *Rosenfeld et al.*, 2008; *Mansell and Ziegler*, 2013; *Zhao et al.*, 2014; *Stolz et al.*, 2015; *Guo et al.*, 2016] AOD in the region of the Indian Ocean shipping lane is typically less than 0.25 and no obvious AOD enhancement is detected over the shipping lane (see SI), consistent with previous studies of shipping effects on aerosols and low-level clouds [*Peters et al.*, 2011]. Aerosols from ship exhaust are small and high rain rates in this specific region lead to efficient CCN removal. Moreover, an enhanced CCN number concentration important for cloud microphysics may be a nearly undetectable AOD enhancement, especially in relatively clean regions with low CCN. As such, using AOD and/or orbiting lightning sensors with infrequent sampling of any one region may miss the effects of aerosol particle enhancements in relatively clean environments, [*Peters et al.*, 2011] which are where the sensitivity of the cloud microphysics, convection, and lightning to aerosol may in fact be highest.[*Ramanathan et al.*, 2001; *Williams et al.*, 2002; *Rosenfeld et al.*, 2008; *Stolz et al.*, 2015] In this way, the enhanced lightning we observe directly over the shipping lanes indicates a uniquely isolated and persistent perturbation experiment of otherwise relatively clean marine convective systems.

We note that the two shipping lanes presented herein have the most obvious lightning enhancements detectable with the long record of lightning strokes provided at high time and spatial resolution by WWLLN. Other shipping lanes do not have the same intensity of emissions, so that the enhancement of aerosol particles and precursors is smaller, and some lanes are in regions where there is either little convection or where the continental influence overwhelms the shipping-induced aerosol effects on convective invigoration and

electrification. That said, a thorough analysis of each of the world's major shipping lanes is warranted, as are *in situ* studies to better constrain the actual perturbation to CCN within the regions of the most remote and busiest shipping lanes.

Summary and Conclusions

Storm intensification has obvious consequences for human life and the global economy through damages from wind and hail, as well as from direct lightning strikes. We find lightning frequency to be enhanced by a factor of about two on an annual basis centered over two of the world's main shipping lanes. Meteorological factors are unable to explain these enhancements and we conclude that aerosol particles resulting from shipping emissions perturb cloud microphysics, convection, and ice processes leading to enhanced lightning. The localized and persistent nature of the enhancement provides a unique, albeit unintentional, opportunity to better quantify the response of storm intensity and lightning to changes in aerosol particles caused by human activities. Our findings suggest that even small absolute increases in remote marine aerosol particles due to human activities could have a substantial impact on storm intensity and lightning. As such, there have likely been increases in storm vertical development and lightning in remote regions since the pre-industrial era, which has consequences not only for human life and property, but also for atmospheric composition and climate.

Acknowledgements

The authors thank Earle Williams, James Brundell, Robert Wood, Dale Durran, and an anonymous reviewer for their constructive comments that substantially improved the manuscript. KV was supported by an appointment to the NASA Postdoctoral Program at the Marshall Space Flight Center, administered by Universities Space Research Association

through a contract with NASA. This research was also supported in part by NOAA grant NA15OAR4320063 AM48 to the University of Washington through JISAO (Joint Institute for the Study of Atmosphere and Ocean). We thank the World Wide Lightning Location Network (WWLLN, see http://wwlln.net and also https://webflash.ess.washington.edu/climate/) which is a collaboration among over 50 research institutions around the world. The EDGAR emissions inventory was obtained from the European Commission Joint Research Center (http://edgar.jrc.ec.europa.eu). ERA-Interim data were obtained from the European Centre for Medium-Range Weather Forecasts (http://www.ecmwf.int). TRMM rainfall and lightning data were obtained from Goddard Space Flight Center (http://mirador.gsfc.nasa.gov) and the Global Hydrology Research Center (http://lightning.nsstc.nasa.gov), respectively. CALIPSO aerosol data were obtained from the Atmospheric Data Sciences Center at NASA Langley Research Center (https://eosweb.larc.nasa.gov/project/calipso/aerosol_profile_table). Sea Surface Temperatures were obtained from the NOAA Optimal Interpolation data set (https://climatedataguide.ucar.edu/climate-data/sst-data-noaa-high-resolution-025x025-blended-analysis-daily-sst-and-ice-oisstv2). Port of Singapore statistics were obtained from the Maritime Port Authority (http://www.mpa.gov.sg/). Raw data used for this work are publicly available, and the data tables used to generate Figures 1 – 4 are provided as NetCDF files via the University of Washington Libraries Research Works data archive https://digital.lib.washington.edu/researchworks/.

References:

Abarca, S. F., K. L. Corbosiero, and T. J. G. Jr (2010), An evaluation of the Worldwide Lightning Location Network (WWLLN) using the National Lightning Detection Network (NLDN) as ground truth, *J. Geophys. Res.*, *115*(D18206), 1–11, doi:10.1029/2009JD013411.

Altaratz, O., I. Koren, Y. Yair, and C. Price (2010), Lightning response to smoke from Amazonian fires, *Geophys. Res. Lett.*, *37*(7), 1–6, doi:10.1029/2010GL042679.

Altaratz, O., I. Koren, L. A. Remer, and E. Hirsch (2014), Review: Cloud invigoration by aerosols-Coupling between microphysics and dynamics, *Atmos. Res.*, *140–141*, 38–60, doi:10.1016/j.atmosres.2014.01.009.

Andreae, M. O. (2004), Smoking Rain Clouds over the Amazon, *Science*, *303*(5662), 1337–1342, doi:10.1126/science.1092779.

Banzon, V., and R. Reynolds (2017), The Climate Data Guide: SST data: NOAA High-resolution (0.25x0.25) Blended Analysis of Daily SST and Ice, OISSTv2., Available from: https://climatedataguide.ucar.edu/climate-data/sst-data-noaa-high-resolution-025x025-blended-analysis-daily-sst-and-ice-oisstv2 (Accessed 21 July 2017)

Bell, T. L., D. Rosenfeld, K. M. Kim, J. M. Yoo, M. I. Lee, and M. Hahnenberger (2008), Midweek increase in U.S. summer rain and storm heights suggests air pollution invigorates rainstorms, *J. Geophys. Res. Atmos.*, *113*(2), 1–22, doi:10.1029/2007JD008623.

Bell, T. L., D. Rosenfeld, and K. M. Kim (2009), Weekly cycle of lightning: Evidence of storm invigoration by pollution, *Geophys. Res. Lett.*, *36*(23), 1–5, doi:10.1029/2009GL040915.

Boccippio, D. J., W. J. Koshak, and R. J. Blakeslee (2002), Performance assessment of the optical transient detector and lightning imaging sensor. Part I: Predicted diurnal

variability, *J. Atmos. Ocean. Technol.*, *19*(9), 1318–1332, doi:10.1029/2006JD007787.

Boucher, O., and U. Lohmann (1995), The sulfate- CCN- cloud albedo effect, *Tellus B*, *47*(3), 281–300, doi:10.1034/j.1600-0889.47.issue3.1.x.

Crippa, M., G. Janssens-Maenhout, F. Dentener, D. Guizzardi, K. Sindelarova, M. Muntean, R. Van Dingenen, and C. Granier (2016), Forty years of improvements in European air quality: Regional policy-industry interactions with global impacts, *Atmos. Chem. Phys.*, *16*(6), 3825–3841, doi:10.5194/acp-16-3825-2016.

Curran, E. B., R. L. Holle, and R. E. Lopez (2000), Lightning casualties and damages in the United States from 1959 to 1994, *J. Clim.*, *13*(19), 3448–3464, doi:10.1175/1520-0442(2000)013<3448:LCADIT>2.0.CO;2.

Dee, D. P. et al. (2011), The ERA-Interim reanalysis : configuration and performance of the data assimilation system, *Q. J. R. Meteorol. Soc.*, *137*(April), 553–597, doi:10.1002/qj.828.

Dowden, R. L., J. B. Brundell, and C. J. Rodger (2002), VLF lightning location by time of group arrival (TOGA) at multiple sites, *J. Atmos. Solar-Terrestrial Phys.*, *64*, 817–830.

Dunne, E. M. et al. (2016), Global atmospheric particle formation from CERN CLOUD measurements, *Science*, *354*(6316), 1119–1124, doi:10.1126/science.aaf2649.

Durkee, P. A., R. E. Chartier, A. Brown, E. J. Trehubenko, S. D. Rogerson, C. Skupniewicz, K. E. Nielsen, S. Platnick, and M. D. King (2000), Composite Ship Track Characteristics, *J. Atmos. Sci.*, *57*(16), 2542–2553, doi:10.1175/1520-0469(2000)057<2542:CSTC>2.0.CO;2.

Fan, J., L. R. Leung, D. Rosenfeld, Q. Chen, Z. Li, J. Zhang, and H. Yan (2013), Microphysical effects determine macrophysical response for aerosol impacts on deep convective clouds, *Proc. Natl. Acad. Sci.*, *110*(48), E4581–E4590, doi:10.1073/pnas.1316830110.

Flannigan, M. D., and B. M. Wotton (1991), Lightning-ignited forest fires in northwestern Ontario, *Can. J. For. Res.*, *21*(3), 277–287, doi:10.1139/x91-035.

Galloway, J. N. et al. (2004), Nitrogen cycles: past, present, and future, *Biogeochemistry*, *70*(2), 153–226, doi:DOI 10.1007/s10533-004-0370-0.

Guo, J., M. Deng, S. S. Lee, F. Wang, Z. Li, P. Zhai, H. Liu, W. Lv, W. Yao, and X. Li (2016), Delaying precipitation and lightning by air pollution over the Pearl River Delta. Part I: Observational analyses, *J. Geophys. Res. Atmos.*, *121*(11), 6472–6488, doi:10.1002/2015JD023257.

Heiblum, R. H., I. Koren, and O. Altaratz (2012), New evidence of cloud invigoration from TRMM measurements of rain center of gravity, *Geophys. Res. Lett.*, *39*(8), 1–7, doi:10.1029/2012GL051158.

Hobbs, P. V et al. (2000), Emissions from Ships with respect to Their Effects on Clouds, *J. Atmos. Sci.*, *57*(16), 2570–2590, doi:10.1175/1520-0469(2000)057<2570:EFSWRT>2.0.CO;2.

Huffman, G. J., D. T. Bolvin, E. J. Nelkin, D. B. Wolff, R. F. Adler, G. Gu, Y. Hong, K. P. Bowman, and E. F. Stocker (2007), The TRMM Multisatellite Precipitation Analysis (TMPA): Quasi-Global, Multiyear, Combined-Sensor Precipitation Estimates at Fine Scales, *J. Hydrometeorol.*, *8*(1), 38–55, doi:10.1175/JHM560.1.

Hutchins, M. L., R. H. Holzworth, J. B. Brundell, and C. J. Rodger (2012), Relative detection efficiency of the World Wide Lightning Location Network, *Radio Sci.*, *47*(October), 1–9, doi:10.1029/2012RS005049.

Hutchins, M. L., R. H. Holzworth, K. S. Virts, J. M. Wallace, and S. Heckman (2013), Radiated VLF energy differences of land and oceanic lightning, *Geophys. Res. Lett.*, *40*(10), 2390–2394, doi:10.1002/grl.50406.

Hutchins, M. L., R. H. Holzworth, and J. B. Brundell (2014), Diurnal variation of the global

electric circuit from clustered thunderstorms, *J. Geophys. Res. Sp. Phys.*, *119*, 620–629, doi:10.1002/2013JA019593.

Iguchi, T., T. Kozu, R. Meneghini, J. Awaka, and K. Okamoto (2000), Rain-Profiling Algorithm for the TRMM Precipitation Radar, *J. Appl. Meteorol.*, *39*(12), 2038–2052, doi:10.1175/1520-0450(2001)040<2038:RPAFTT>2.0.CO;2.

Jacobson, A. R., R. Holzworth, J. Harlin, R. Dowden, and E. Lay (2006), Performance assessment of the World Wide Lightning Location Network (WWLLN), using the Los Alamos Sferic Array (LASA) as ground truth, *J. Atmos. Ocean. Technol.*, *23*(8), 1082–1092, doi:10.1175/JTECH1902.1.

Jenkins, G. S., and A. Pratt (2008), Saharan dust, lightning and tropical cyclones in the eastern tropical Atlantic during NAMMA-06, *Geophys. Res. Lett.*, *35*(12), 10–15, doi:10.1029/2008GL033979.

Khain, a., N. Cohen, B. Lynn, and a. Pokrovsky (2008), Possible Aerosol Effects on Lightning Activity and Structure of Hurricanes, *J. Atmos. Sci.*, *65*, 3652–3677, doi:10.1175/2008JAS2678.1.

Koren, I., Y. J. Kaufman, D. Rosenfeld, L. A. Remer, and Y. Rudich (2005), Aerosol invigoration and restructuring of Atlantic convective clouds, *Geophys. Res. Lett.*, *32*(14), 1–4, doi:10.1029/2005GL023187.

Lack, D. A. et al. (2009), Particulate emissions from commercial shipping: Chemical, physical, and optical properties, *J. Geophys. Res. Atmos.*, *114*(4), 1–16, doi:10.1029/2008JD011300.

Lauer, a., V. Eyring, J. Hendricks, P. Jöckel, and U. Lohmann (2007), Global model simulations of the impact of ocean-going ships on aerosols, clouds, and the radiation budget, *Atmos. Chem. Phys. Discuss.*, *7*(4), 9419–9464, doi:10.5194/acpd-7-9419-2007.

Li, Z., F. Niu, J. Fan, Y. Liu, D. Rosenfeld, and Y. Ding (2011), Long-term impacts of

aerosols on the vertical development of clouds and precipitation, *Nat. Geosci.*, *4*(12), 888–894, doi:10.1038/ngeo1313.

Logan, J. A. (1983), Nitrogen oxides in the trophosphere: global and regional budgets., *J. Geophys. Res.*, *88*(1), 10785–10807, doi:doi:10.1029/JC088iC15p10785.

Lucas, C., E. J. Zipser, and M. A. Lemone (1994), Convective Available Potential Energy in the Environment of Oceanic and Continental Clouds: Correction and Comments, *J. Atmos. Sci.*, *51*(24), 3829–3830, doi:10.1175/1520-0469(1996)053<1209:COAPEI>2.0.CO;2.

Mansell, E. R., and C. L. Ziegler (2013), Aerosol Effects on Simulated Storm Electrification and Precipitation in a Two-Moment Bulk Microphysics Model, *J. Atmos. Sci.*, *70*(7), 2032–2050, doi:10.1175/JAS-D-12-0264.1.

Merikanto, J., D. V. Spracklen, G. W. Mann, S. J. Pickering, and K. S. Carslaw (2009), Impact of nucleation on global CCN, *Atmos. Chem. Phys.*, *9*(21), 8601–8616, doi:10.5194/acp-9-8601-2009.

Mickley, L. J., D. J. Jacob, and D. Rind (2001), Uncertainty in preindustrial abundance of tropospheric ozone: Implications for radiative forcing calculations, *J. Geophys. Res.*, *106*(D4), 3389–3399, doi:10.1029/2000JD900594.

Peters, K., J. Quaas, and H. Graßl (2011), A search for large-scale effects of ship emissions on clouds and radiation in satellite data, *J. Geophys. Res. Atmos.*, *116*(24), 1–20, doi:10.1029/2011JD016531.

Pierce, J. R., K. Chen, and P. J. Adams (2007), Contribution of carbonaceous aerosol to cloud condensation nuclei: processes and uncertainties evaluated with a global aerosol microphysics model, *Atmos. Chem. Phys. Discuss.*, *7*(3), 7723–7765, doi:10.5194/acpd-7-7723-2007.

Price, C., J. Penner, and M. Prather (1997), NOx from lightning: 1. Global distribution based

on lightning physics, *J. Geophys. Res.*, *102*, 5929, doi:10.1029/96JD03504.

Ramanathan, V., P. J. Crutzen, J. T. Kiehl, and D. Rosenfeld (2001), Aerosol, climate, and the hydrological cycle, *Science*, *294*(5549), 2119–2124, doi:10.1126/science.1064034.

Remer, L. A. et al. (2008), Global aerosol climatology from the MODIS satellite sensors, *J. Geophys. Res. Atmos.*, *113*(14), 1–18, doi:10.1029/2007JD009661.

Reynolds, R. W., T. M. Smith, C. Liu, D. B. Chelton, K. S. Casey, and M. G. Schlax (2007), Daily high-resolution-blended analyses for sea surface temperature, *J. Clim.*, *20*(22), 5473–5496, doi:10.1175/2007JCLI1824.1.

Reynolds, S. E., M. Brook, and M. F. Gourley (1957), Thunderstorm Charge Separation, *J. Meteorol.*, *14*(5), 426–436, doi:10.1175/1520-0469(1957)014<0426:TCS>2.0.CO;2.

Rodger, C. J., S. Werner, J. B. Brundell, E. H. Lay, N. R. Thomson, R. H. Holzworth, and R. L. Dowden (2006), Detection efficiency of the VLF World-Wide Lightning Location Network (WWLLN): initial case study, *Ann. Geophys.*, *24*(12), 3197–3214, doi:10.5194/angeo-24-3197-2006.

Rorig, M. L., and S. a. Ferguson (1999), Characteristics of Lightning and Wildland Fire Ignition in the Pacific Northwest, *J. Appl. Meteorol.*, *38*(1986), 1565–1575, doi:10.1175/1520-0450(1999)038<1565:COLAWF>2.0.CO;2.

Rosenfeld, D. (2000), Suppression of Rain and Snow by Urban and Industrial Air Pollution, *Science*, *287*(5459), 1793–1796, doi:10.1126/science.287.5459.1793.

Rosenfeld, D., and W. Woodley (2000), Deep convective clouds with sustained supercooled liquid water down to -37.5 degrees C, *Nature*, *405*(6785), 440–2, doi:10.1038/35013030.

Rosenfeld, D., U. Lohmann, G. B. Raga, C. D. O'Dowd, M. Kulmala, S. Fuzzi, A. Reissell, and M. O. Andreae (2008), Flood or Drought: How Do Aerosols Affect Precipitation?, *Science*, *321*(5894), 1309–1313, doi:10.1126/science.1160606.

Rosenfeld, D. et al. (2014), Global observations of aerosol-cloud-precipitation- climate interactions, *Rev. Geophys*, *52*, 750–808, doi:10.1002/2013RG000441.

Seiler, W., and P. J. Crutzen (1980), Estimates of gross and net fluxes of carbon between the biosphere and the atmosphere from biomass burning, *Clim. Change*, *2*(3), 207–247, doi:10.1007/BF00137988.

Sherwood, S. C., V. T. J. Phillips, and J. S. Wettlaufer (2006), Small ice crystals and the climatology of lightning, *Geophys. Res. Lett.*, *33*(5), 2–5, doi:10.1029/2005GL025242.

Smith, T. W. P. et al. (2014), Third IMO Greenhouse Gas Study 2014, *Int. Marit. Organ.*, 327, doi:10.1007/s10584-013-0912-3, see also www.shipmap.org.

Stevenson, D. S. et al. (2013), Tropospheric ozone changes, radiative forcing and attribution to emissions in the Atmospheric Chemistry and Climate Model Intercomparison Project (ACCMIP), *Atmos. Chem. Phys.*, *13*(6), 3063–3085, doi:10.5194/acp-13-3063-2013.

Stolz, D. C., S. A. Rutledge, and J. R. Pierce (2015), Simultaneous influences of thermodynamics and aerosols on deep convection and lightning in the tropics, *J. Geophys. Res. Atmos.*, *120*(12), 6207–6231, doi:10.1002/2014JD023033.

Storer, R. L., S. C. Van Den Heever, and T. S. L'Ecuyer (2014), Observations of aerosol-induced convective invigoration in the tropical east Atlantic, *J. Geophys. Res.*, *119*(7), 3963–3975, doi:10.1002/2013JD020272.

Twohy, C. H., P. A. Durkee, B. J. Huebert, and R. J. Charlson (1995), Effects of aerosol particles on the microphysics of coastal stratiform clouds, *J. Clim.*, *8*(4), 773–783, doi:10.1175/1520-0442(1995)008<0773:EOAPOT>2.0.CO;2.

Virts, K. S., J. M. Wallace, M. L. Hutchins, and R. H. Holzworth (2013), Highlights of a new ground-based, hourly global lightning climatology, *Bull. Am. Meteorol. Soc.*, *94*(9), 1381–1391, doi:10.1175/BAMS-D-12-00082.1.

Voropayev, S. I., C. Nath, and H. J. S. Fernando (2012), Thermal surface signatures of ship

propeller wakes in stratified waters, *Phys. Fluids*, *24*(11), doi:10.1063/1.4767130.

Waliser, D. E., and C. Gautier (1993), A satellite-derived climatology of the ITCZ, *J. Clim.*, *6*(11), 2162–2174, doi:10.1175/1520-0442(1993)006<2162:ASDCOT>2.0.CO;2.

Wall, C., E. Zipser, and C. Liu (2014), An Investigation of the Aerosol Indirect Effect on Convective Intensity Using Satellite Observations, *J. Atmos. Sci.*, *71*(1), 430–447, doi:10.1175/JAS-D-13-0158.1.

Wang, Y., M. Wang, R. Zhang, S. J. Ghan, Y. Lin, J. Hu, B. Pan, M. Levy, J. H. Jiang, and M. J. Molina (2014), Assessing the effects of anthropogenic aerosols on Pacific storm track using a multiscale global climate model, *Proc. Natl. Acad. Sci.*, *111*(19), 6894–6899, doi:10.1073/pnas.1403364111.

Williams, E., and S. Stanfill (2002), The physical origin of the land-ocean contrast in lightning activity, *Comptes Rendus Phys.*, *3*(10), 1277–1292, doi:10.1016/S1631-0705(02)01407-X.

Williams, E. et al. (2002), Contrasting convective regimes over the Amazon: Implications for cloud electrification, *J. Geophys. Res.*, *107*(D20), 8082, doi:10.1029/2001JD000380.

Williams, E. R. (2005), Lightning and climate: A review, *Atmos. Res.*, *76*, 272–287, doi:10.1016/j.atmosres.2004.11.014.

Winker, D. M., W. H. Hunt, and M. J. McGill (2007), Initial performance assessment of CALIOP, *Geophys. Res. Lett.*, *34*(19), 1–5, doi:10.1029/2007GL030135.

Yuan, T., L. A. Remer, K. E. Pickering, and H. Yu (2011), Observational evidence of aerosol enhancement of lightning activity and convective invigoration, *Geophys. Res. Lett.*, *38*(4), 1–5, doi:10.1029/2010GL046052.

Zhao, P., Y. Yin, and H. Xiao (2014), The effects of aerosol on development of thunderstorm electrification: A simulation study in Weather Research and Forecasting (WRF) model, *2014 Int. Conf. Light. Prot. ICLP 2014*, *153*, 177–180, doi:10.1109/ICLP.2014.6973116.

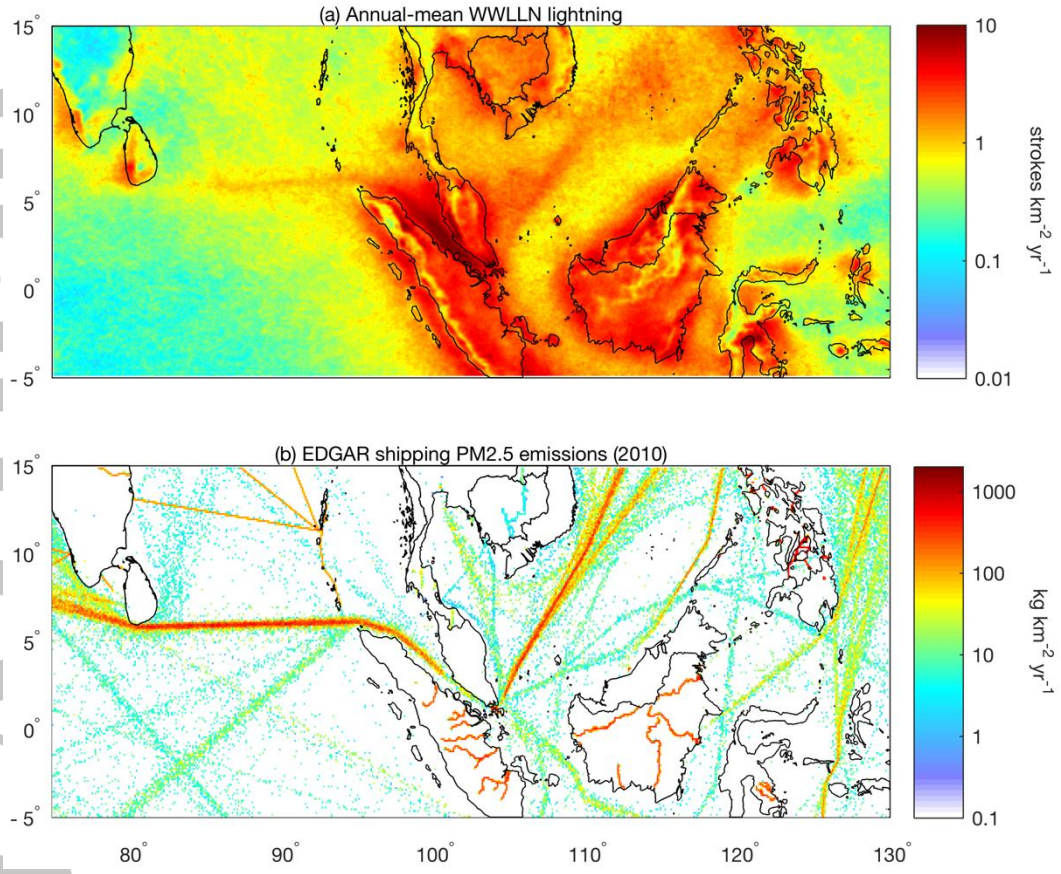

Figure 1: (a) Observed annual-mean WWLLN lightning density for 2005-16 in the eastern Indian Ocean and the South China Sea. (b) $PM_{2.5}$ shipping emissions estimates from EDGAR database for 2010, both at 0.1° resolution. See text and SI for more details.

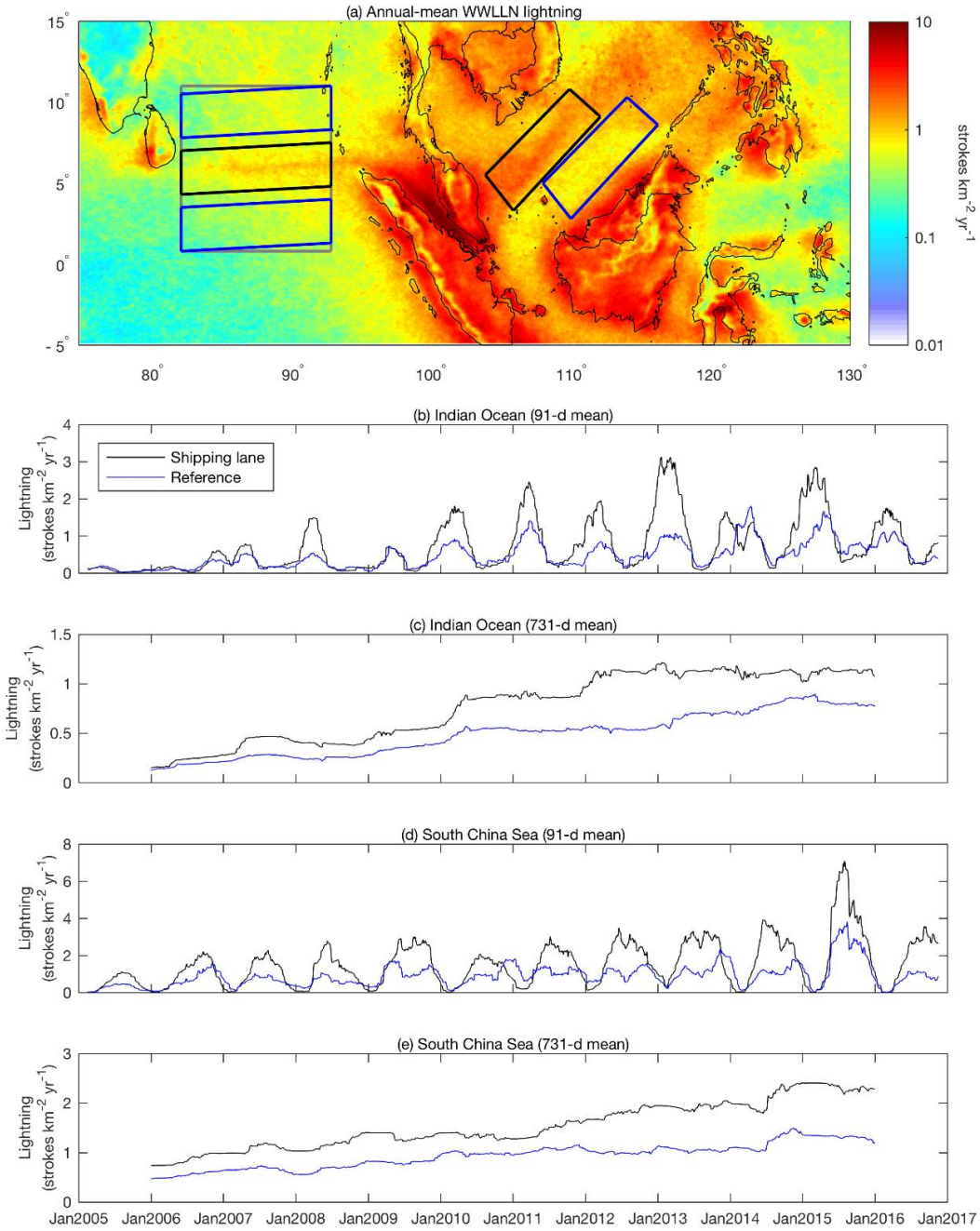

Figure 2. (a) As in Fig. 1a, with polygons for the shipping lanes (black), the reference regions (blue), and the averaging region used in Fig. 3 (gray). (b, c) 91- and 731-day running mean time series of WWLLN lightning density averaged over the Indian Ocean shipping lane (black) and the northern and southern reference regions (blue). (d, e) As in (b, c), but for the South China Sea shipping lane and single reference region.

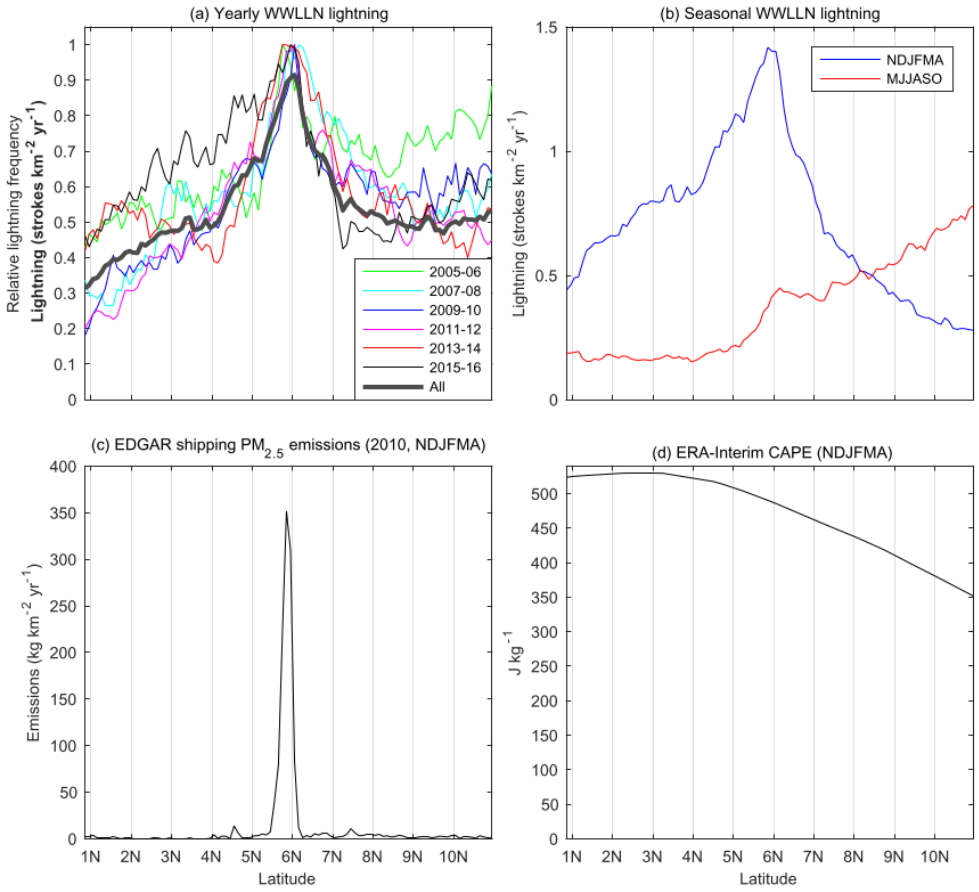

Figure 3. (a) WWLLN lightning density over the Indian Ocean shipping lane (gray box in Fig. 2a) averaged zonally at 0.1º intervals for two-year periods and normalized relative to the maximum frequency of the two-year average (thin lines). Absolute WWLLN lightning density (strokes km^{-2} yr^{-1}) zonally averaged as for the two-year averages but including all years (2005-2016) is shown as the thick black line. (b) As in (a), but with data averaged seasonally for November – April (NDJFMA) and May – October (MJJASO). (c) Zonal-mean EDGAR $PM_{2.5}$ shipping emissions for NDJFMA (emissions change by only 10% across the year) during the year 2010. (d) ERA-Interim Convective Available Potential Energy across the same region averaged seasonally for NDJFMA (when the lightning enhancement is largest) from 2005 to 2016.

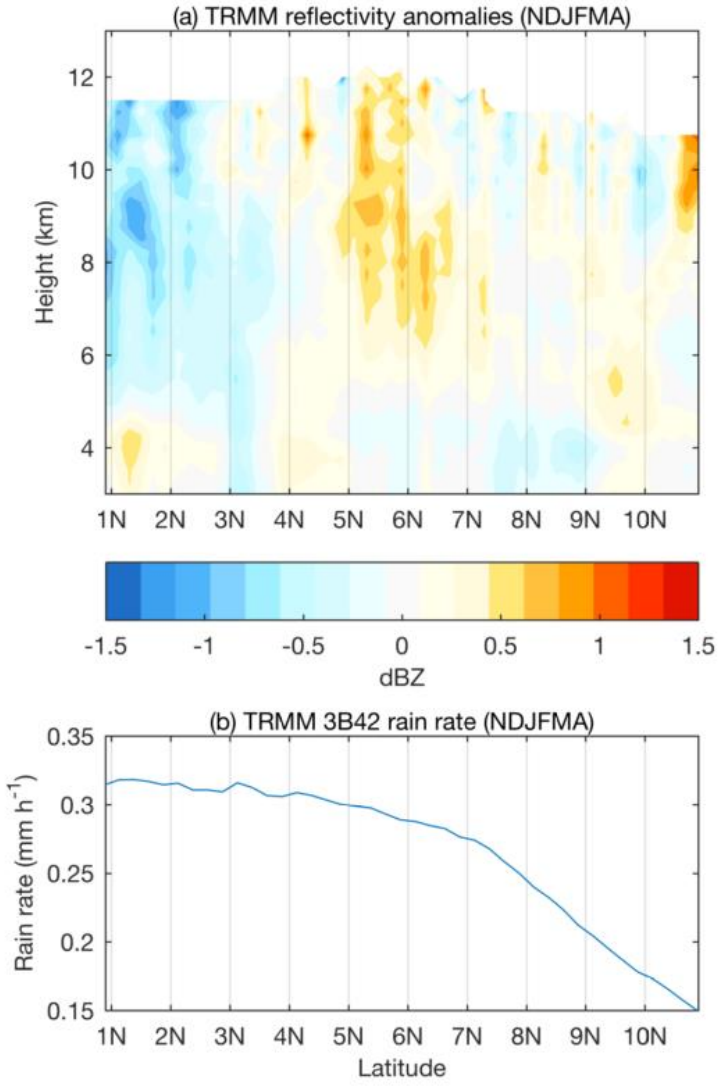

Figure 4. Top: Zonal-mean TRMM radar reflectivity anomalies (dBZ) for November – April (NDJFMA) as a function of altitude over the same region shown in Figure 3. Mean reflectivity in the region at each height was calculated for NDJFMA over the full TRMM record (1998 – 2015), then subtracted from the mean reflectivity at each 0.2° latitude bin. Only TRMM profiles flagged as containing rain were included, and only points sampled by >1000 profiles are shown. Bottom: zonal-mean rain rate from the 3-hourly gridded TRMM 3B42 dataset for November – April across the same time-period and region as in the top panel.